



ÉCOLE POLYTECHNIQUE DE LOUVAIN

LELEC2710 - NANOELECTRONICS

**Imaging magnetic focusing of coherent
electron waves**

ARIB Sofiane 22611700
TRINQUET Victor 28021700

With the help of Nicolas Moreau and Pauline de Crombrugghe

Academic year 2021 - 2022

Contents

1	Introduction	2
2	Definition of the system	3
3	Physics of the project	4
3.1	Resonant magnetic field	4
3.2	Scanning gate microscope	4
3.2.1	Working principle	4
3.2.2	Interference fringes	5
3.3	Hopping parameter	5
3.4	Modes in the leads	6
4	System without disorder - 1 mode in the QPCs	8
4.1	Transmission as a function of the magnetic field	8
4.2	SGM images	9
4.2.1	First resonance - $B = 2.40\text{ T}$	9
4.2.2	Second resonance - $B = 4.94\text{ T}$	13
5	System without disorder - 2 modes in the QPCs	14
5.1	Transmission as a function of the magnetic field	14
5.2	SGM images	15
5.2.1	First resonance - $B = 3.53\text{ T}$	15
5.2.2	Second resonance - $B = 7.22\text{ T}$	16
5.2.3	Current Maps	17
6	System with disorder - 1 mode in the QPCs	19
6.1	Transmission as a function of the magnetic field	20
6.2	SGM images	20
6.2.1	First resonance - $B = 2.52\text{ T}$	20
6.2.2	Second resonance - $B = 5.03\text{ T}$	21
7	Conclusion	23

1 Introduction

In the field of nanoelectronics, it can be a real asset to image the electron motion in the system of interest. In that regard, scanning gate microscopes (SGM) were developed and can give valuable insights into the physics at play. However, under a magnetic field, the time-reversal symmetry is broken which implies that the electrons can no longer return to the quantum point contact (QPC) from which they emerged. This leads to a strong decrease of intensity and it becomes impossible to image the outgoing flow of electrons. To solve this issue, one can use a second QPC in order to collect the outgoing electrons from the first one and image their paths via a probe acting as a deflecting lens. By doing so, a shadow is cast downstream and the drop of transmission between the two QPCs is linked to the flow of electrons [1].

The goal of this project was to re-create thanks to the open-source Python package *Kwant* some situations presented in [1]. Figure 1.1 shows the type of results we were ideally aiming at.

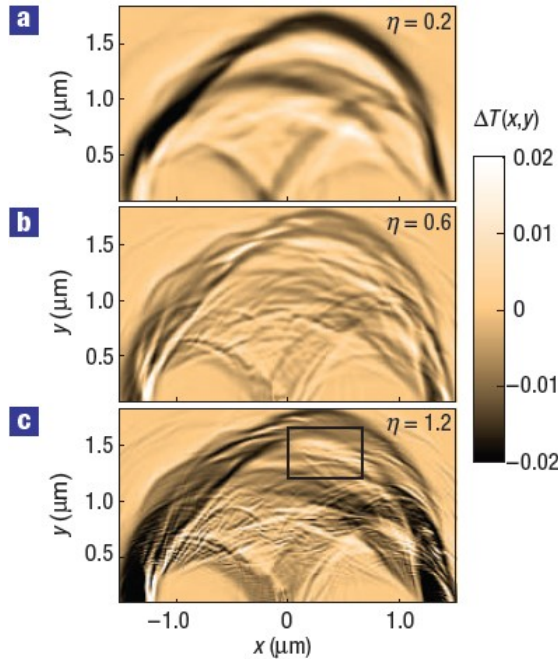


Figure 1.1: Quantum simulations of SPM images including small-angle scattering. ΔT corresponds to the change in transmission between the two QPCs while η describes the strength of the probe. From [1].

This report is articulated as follows. Firstly, the chosen system is exposed as well as the necessary parameters. Secondly, the main physical concepts needed to predict beforehand the simulations and to interpret them are explained. Thirdly, our results are presented and described for various cases. Some theories about unexpected or expected features are given when possible. The following *Github* repository contains all the images shown in this report as well as the video of the current maps with increasing magnetic fields.

<https://github.com/VicTrqt/LELEC2710---Nanoelectronics---Project-Aidala>

2 Definition of the system

A real system is made of too many atoms to be simulated. Starting from this fact, there are two possibilities : either working with a scaling parameter or working with a system made of a smaller number of atoms but still large enough to reproduce physical results. The first possibility allows to increase the scaling parameter up to a factor 10 and leads to many complications. Given that this solution still takes a lot of time for computing results and due to the fact that a schedule must be respected, the second solution has been preferred. The main drawback of the second option is the need for plausible dimensions.

The system is schematically presented in Figure 2.1. Many systems have been tested. The parameters that have been retained are :

- the length of the system $L = 250 \text{ nm}$
- the width of the system $w = 160 \text{ nm}$
- the width of the QPCs $q = 20 \text{ nm}$
- the distance between the two QPCs $d = 120 \text{ nm}$
- the lattice parameter $a = 1 \text{ nm}$
- the hopping parameter $t = 1 \text{ eV}$

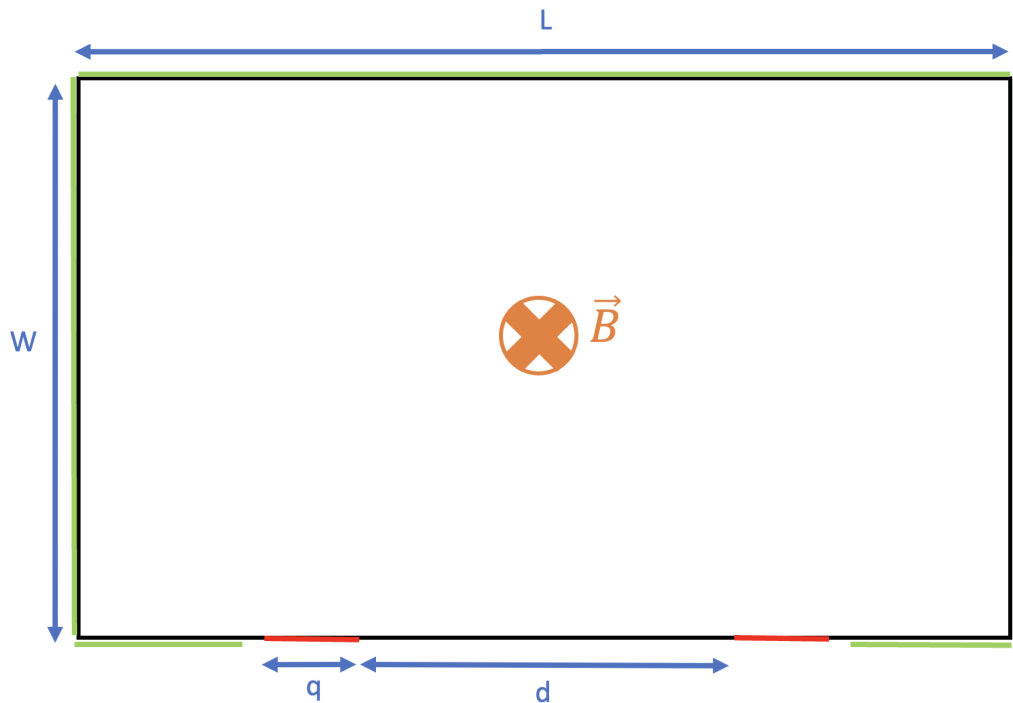


Figure 2.1: Schematics of the system. The green bars are the "vacuum" leads, the red bars are the QPCs, the black bar is the sidewall, and \vec{B} is the uniform magnetic field applied to the system.

3 Physics of the project

3.1 Resonant magnetic field

The cyclotron radius of an electron inside a uniform magnetic field is given by

$$r_c = \frac{\hbar k_F}{eB}, \quad (3.1)$$

where k_F is the Fermi wavevector, e is the absolute value of the charge of the electron, and B is the uniform magnetic field applied to the system. Magnetic focusing occurs when the cyclotron diameter ($2 \cdot r_c$) is a multiple of the distance separating the two QPCs, that is

$$r_c = \frac{d}{2n} \quad (3.2)$$

where n is an integer number. Using the parabolic approximation $E_F = \hbar^2 k_F^2 / 2m^*$ and the effective mass $m^* = \hbar^2 / 2a^2 t$ in the framework of the tight-binding model, the resonant magnetic fields are found to be

$$B_n = n \frac{2\hbar}{ed} \sqrt{\frac{E_F}{t}}. \quad (3.3)$$

Although the resonances found through the simulations may slightly differ, this estimation gives an idea of the expected magnetic fields that should be applied to the system.

3.2 Scanning gate microscope

3.2.1 Working principle

A scanning gate microscope (SGM) uses a charged tip that will deflect the electrons in a system for which the transmission can be measured, for example with a lead on the left from which the electrons come and another lead on the right that collects the electrons.

Schematically, the tip is a movable obstacle in the path of the electrons that is able to change the transmission of the system. If the tip is located at a point where a lot of electrons, reaching the other side of the system, are passing, a large drop in transmission will be measured. Conversely, if the tip is located at a point where only a few electrons are passing, then only a small drop in transmission will be measured.

There is actually another case. The tip can also deflect electrons that were initially coming back into the left lead (or at least not in the right lead if many leads are present in the system) towards the lead on the right. This result is thus an increase in transmission and one can speak of "re-focusing".

There are two steps to follow in order to obtain an image. In a first time, an experiment measuring the conductivity between two leads must be performed in order to obtain the transmission of the system without the tip. In a second time, the tip is raster scanned above the surface and the transmission is measured at each position. Taking the difference $\Delta T = T_{\text{Tip}} - T_{\text{noTip}}$ and mapping

it at each position, one is able to obtain an image giving information about the charges transport in the device.

3.2.2 Interference fringes

If the tip is strong enough, interference fringes are observed on the SGM images [1].

The presence of the tip in the system creates some paths and destroys others. As schematized in Figure 3.1, these created paths can interfere with the original trajectories, leading to an interference pattern that can be seen in the SGM images.

This can be explained by considering that the original trajectories and the trajectories deflected by the tip and reaching the target QPC are interfering with each other at this QPC. The original trajectory contribute with an amplitude $A_0 e^{i\phi_0}$ while the deflected trajectories contribute with an amplitude $A e^{i\phi}$. Therefore the change in transmission depends on the phase difference $\Delta T \propto \cos(\phi - \phi_0)$. When the tip is moved, the phase ϕ changes too. Knowing that $\phi = S/\hbar$, the fringe spacing is found to be

$$d_f = \frac{\lambda_F}{2} \operatorname{cosec} \left(\frac{\theta}{2} \right) \quad (3.4)$$

where θ is the angle of deflection of the trajectory by the tip. When the strength of the tip is increased, the angle of deflection is increased. Hence, according to Equation 3.4, the fringe spacing decreases when the strength of the tip is increased. For a strength $\eta = V/E_F = 1$, the 2DEG is depleted under the tip allowing for backscattering $\theta = 180^\circ$. In this case, the fringe spacing is equal to $\lambda_F/2$ which is the smallest allowed value.

3.3 Hopping parameter

In order to take into account the magnetic field in a tight-binding system, the hopping parameter is modified as,

$$t_{ij}(\vec{A}) = -t \exp \left(\frac{ie}{\hbar} \int_{\vec{R}_i}^{\vec{R}_j} \vec{A} \cdot d\vec{r} \right) \quad (3.5)$$

where \vec{A} is the vector potential, \vec{R}_i is the position of the atom i , and \vec{R}_j is the position of the atom j . For having a clockwise cyclotron orbit, the applied magnetic field must point inside the screen (Figure 2.1) while the \hat{z} axis points towards the reader. Hence, $\vec{B}_z = (0, 0, -B_z)$ with $B_z > 0$. Taking the gauge $\vec{A} = (0, -B_z x, 0)$ ¹, the hopping parameter becomes

$$t_{ij}(B_z) = -t \exp \left(\frac{ie}{\hbar} \int_{y_i}^{y_j} -B_z x dy \right), \quad (3.6)$$

$$= -t \exp \left(\frac{ie}{\hbar} B_z \frac{x_i + x_j}{2} (y_i - y_j) \right) \quad (3.7)$$

where $x = (x_i + x_j)/2$ is the mean between the two atomic positions.

¹ $\vec{\nabla} \times \vec{A} = \frac{\partial}{\partial x}(-B_z x)\hat{z} - \frac{\partial}{\partial z}(-B_z x)\hat{x} = -B_z \hat{z}$ for a uniform magnetic field B_z .

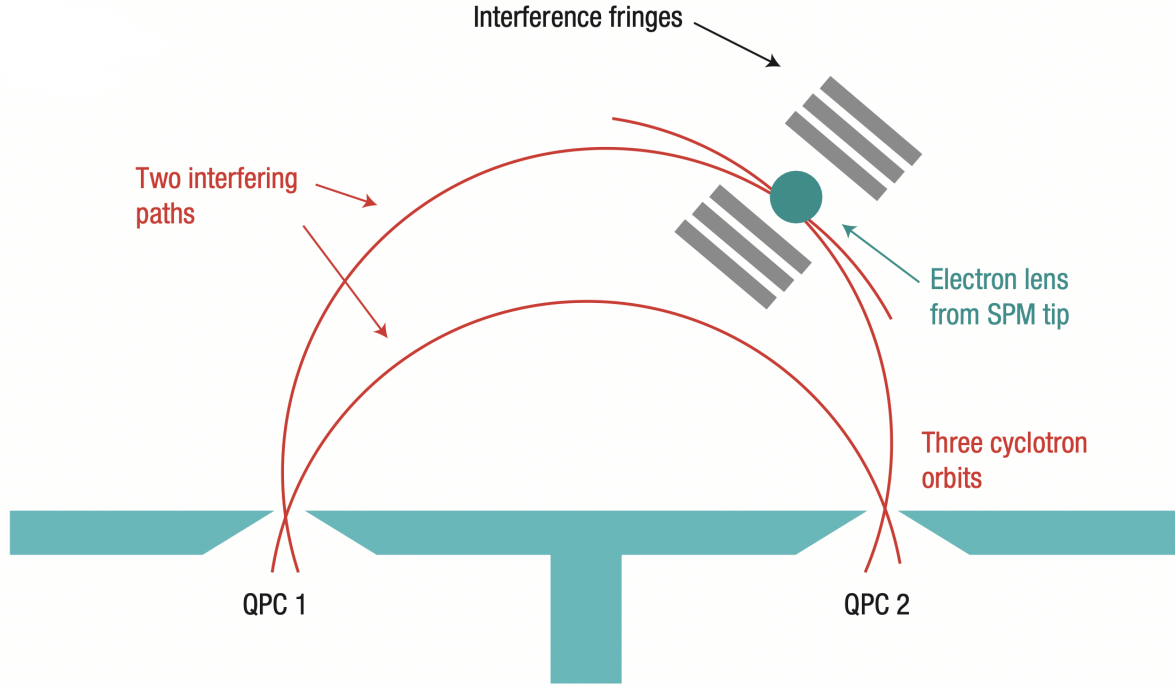


Figure 3.1: Schematics of the two interfering paths arising from the presence of the tip. Interference fringes are also represented, parallel to the trajectory of the electrons [1].

3.4 Modes in the leads

By plotting the band structure of the leads representing the two QPCs, the Fermi level can be adjusted in order to allow a specific number of modes in the leads (see Figure 3.2). This was repeated both with and without the maximum magnetic field so that the number of allowed modes would not change when applying this maximal value.

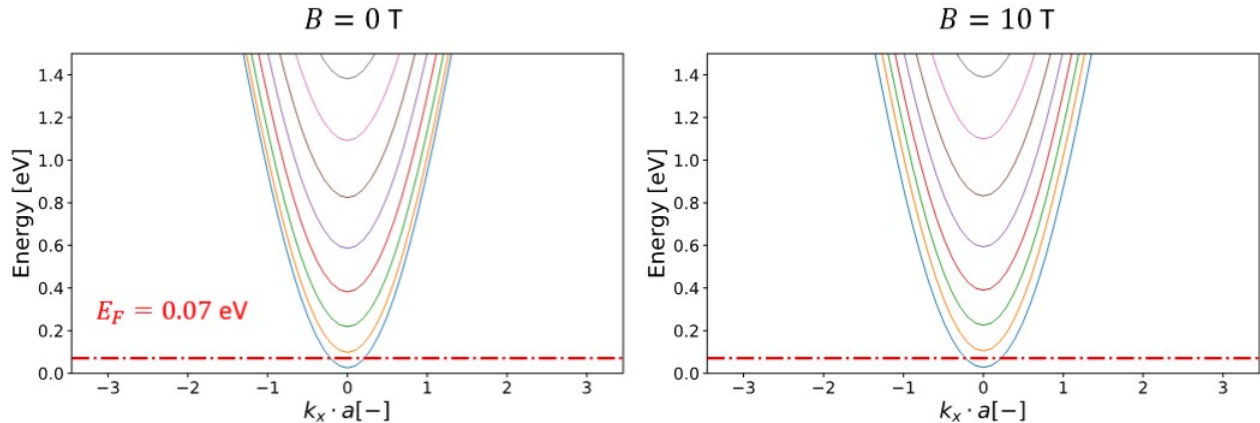


Figure 3.2: Band structure of the two leads representing the QPCs. E_F is the Fermi level and is chosen to allow only 1 mode in this case.

As multiple modes can lead to supplementary interferences, it was decided to start with a unique mode and only afterwards to investigate the effect of an additional one. To that goal, the number

of modes as a function of the Fermi level for zero field and for the maximal one was computed. As shown in Figure 3.3, this helps greatly in choosing the right Fermi level for the desired number of modes. It works less by trials and errors than the previous process.

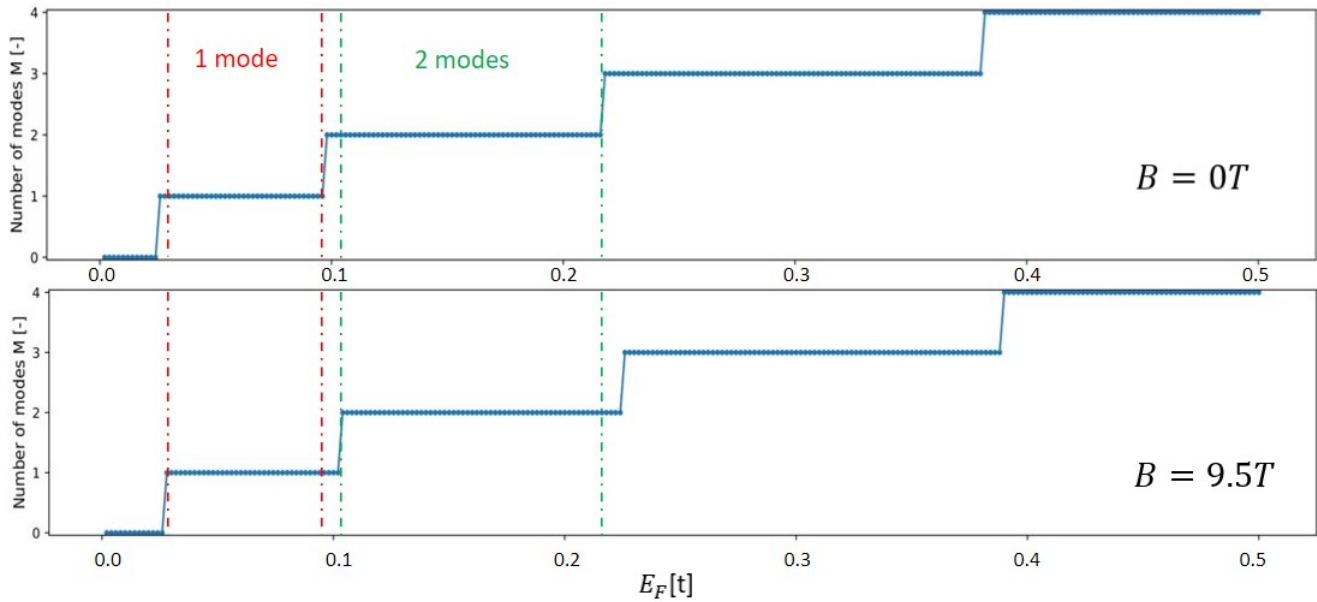


Figure 3.3: Number of modes in the QPCs-leads as a function of the Fermi level in units of the hopping parameter.

4 System without disorder - 1 mode in the QPCs

The system without disorder and only 1 mode allowed in the QPCs is studied. This is realised by choosing the following Fermi level: $E_F = 0.07t$. Although the real system obviously presents some disorder, this first step allows to understand the behavior of the electrons in the system. The first step will be to study the transmission as a function of the magnetic field, in order to localize the two first resonant magnetic fields found by *Kwant*. The second step is to produce SGM images at these resonant magnetic fields in order to observe the classical cyclotron orbit path and the interferences arising from the presence of the tip.

4.1 Transmission as a function of the magnetic field

Figure 4.1 plots the transmission when the magnetic field is varied from 0 T to 7.3 T. Two peaks are visible at 2.40 T and 4.94 T. They are associated to the two first resonances and will be studied in the following sections. Although not being equal to the estimated resonant fields, they respect quite well the fact that the second resonant magnetic field must be twice as large as the first resonant magnetic field, that is $B_2 = 2 \cdot B_1$ (see Equation 3.3). This suggests that one should just multiply by a factor the estimations computed with Equation 3.3 in order to be correct. This factor is found to be 0.839 by taking the average correction of B_1 and B_2 .

The reflection inside the left QPC and the transmission in the other leads are also plotted. The results may look evident, there is no reflection and the electrons which are not going in the right QPC are going in the other leads. However, this is not the case if the hopping is not well defined in the system which can lead to an important reflection in the left QPC, leading to the absence of electrons in the system for large enough fields.

A video of the current map with increasing magnetic field in this situation can be found at https://github.com/VicTrqt/LELEC2710---Nanoelectronics---Project-Aidala/blob/main/1%20Mode/Video_NoDisorder_1mode.avi.

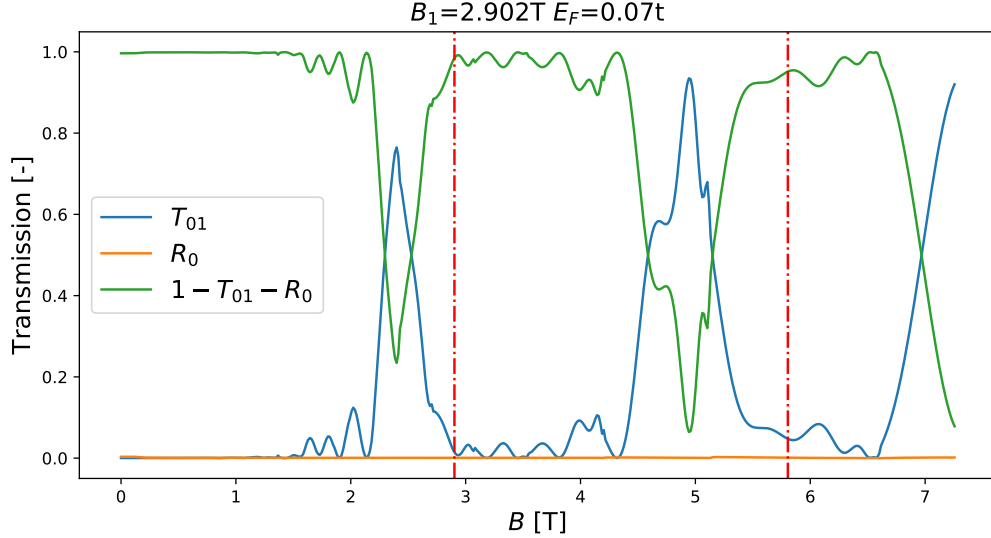


Figure 4.1: Transmission from the first to the second QPC, T_{01} as a function of the magnetic field for a system without disorder and 1 mode in the QPCs. The reflection inside the left QPC, R_0 , and the transmission in the other leads, $1 - T_{01} - R_0$, are also represented. The theoretically calculated resonant magnetic fields are represented by the vertical dot-and-dashed red lines. B_1 in the title is the first resonant magnetic field computed with Equation 3.3.

4.2 SGM images

In order to create the SGM images, a tip is raster scanned at the surface of the sample. In *Kwant*, the tip is introduced by changing the onsite energy. The closer the site to the tip, the stronger the influence of the potential on its onsite energy. The potential of the tip V_t has a gaussian shape expressed as

$$V_t = V \exp\left(\frac{-r^2}{2w_t^2}\right) \quad (4.1)$$

where w_t is the width of the tip (which represents the standard deviation of the distribution) and r is the distance between the considered site and the position of the tip, expressed as

$$r = \sqrt{(x - x_{\text{tip}})^2 + (y - y_{\text{tip}})^2} \quad (4.2)$$

where x and y give the position of the site while x_{tip} and y_{tip} give the position of the tip.

4.2.1 First resonance - $B = 2.40\text{T}$

Variation of the tip width with $\eta = 0.2$ The influence of the tip width with a weak tip can be observed in Figure 4.2.

When the tip is very small (2 nm), the difference of transmission compared to the case without tip is very small (10^{-2}). This is in agreement with the intuition, telling that a small tip will not be able to deflect many electrons. More quantitatively, the Fermi wavelength $\lambda_F = 2\pi a\sqrt{t/E_F} =$

23.75 nm is much larger than the width of the tip, meaning the electrons almost do not "see" the tip. The small tip allows to observe interferences perpendicular to the classical cyclotron with a good contrast. Although the physical origin of these interferences is unclear, it is admitted that the tip must play role. Otherwise, there would not be any image.

When the size of the tip is increased, the difference of transmission increases. The visibility of the interferences decreases but the classical cyclotron orbit becomes distinguishable. Indeed, the electrons are now able to "see" the potential of the tip which is still $\sim 0.1 \cdot V$ at a distance of 24 nm.

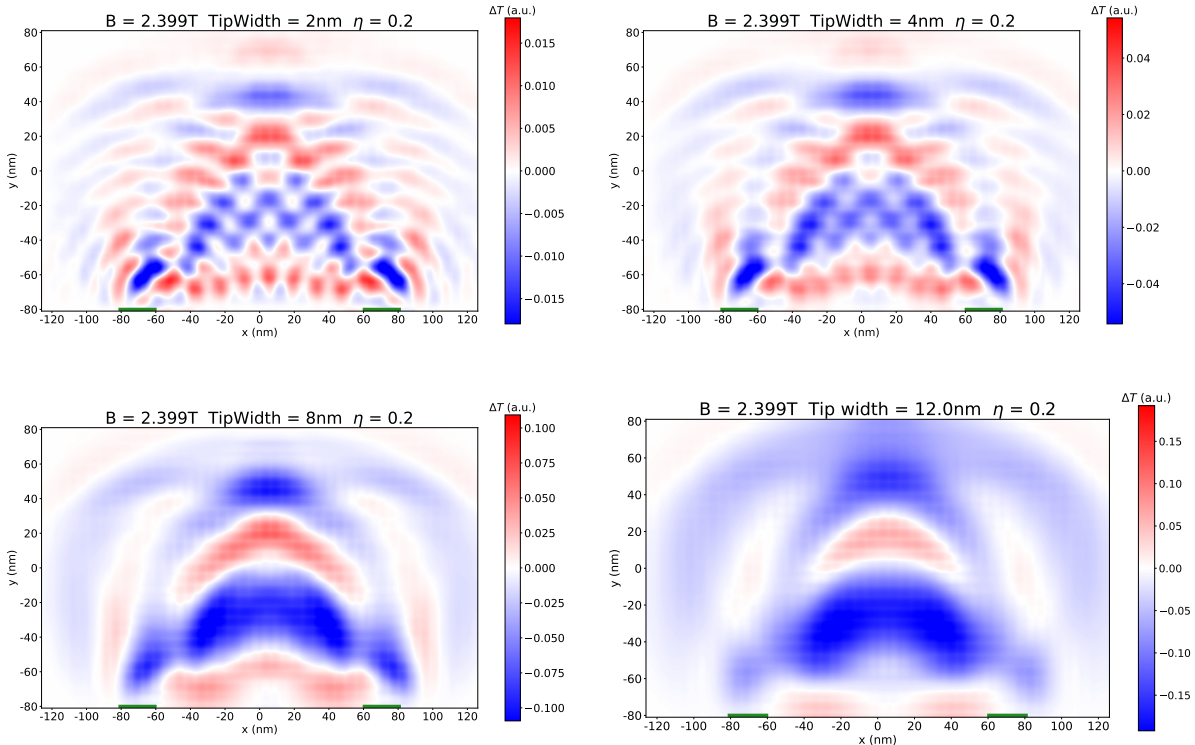


Figure 4.2: One mode - first resonance - $\eta = 0.2$ - variation of the tip width.

Variation of the tip width with $\eta = 1.2$ The influence of the tip width with a strong tip can be observed in Figure 4.3.

When the size of the tip is very small, the transmission is relatively small, as expected. In a similar way to the weak tip, the interferences are more visible with the very small tip although the cyclotron orbit is more visible than its counterpart in Figure 4.2.

When the size of the tip is increased, it is clear that the tip becomes very bad at refocusing since the difference of transmission is negative almost everywhere on the map. This can be explained by the apparition of electrons backscattering for a strong tip. Indeed, $\eta \geq 1$ allows the tip to scatter the electrons with an angle of 180° , thus destroying a lot of paths that were going into the right QPC. This backscattering also explains why the fringes of interference are more visible with a strong tip; the backscattered electron interferes with itself, sometimes destructively and other times constructively, with a fringe spacing given by $\lambda_F/2$.

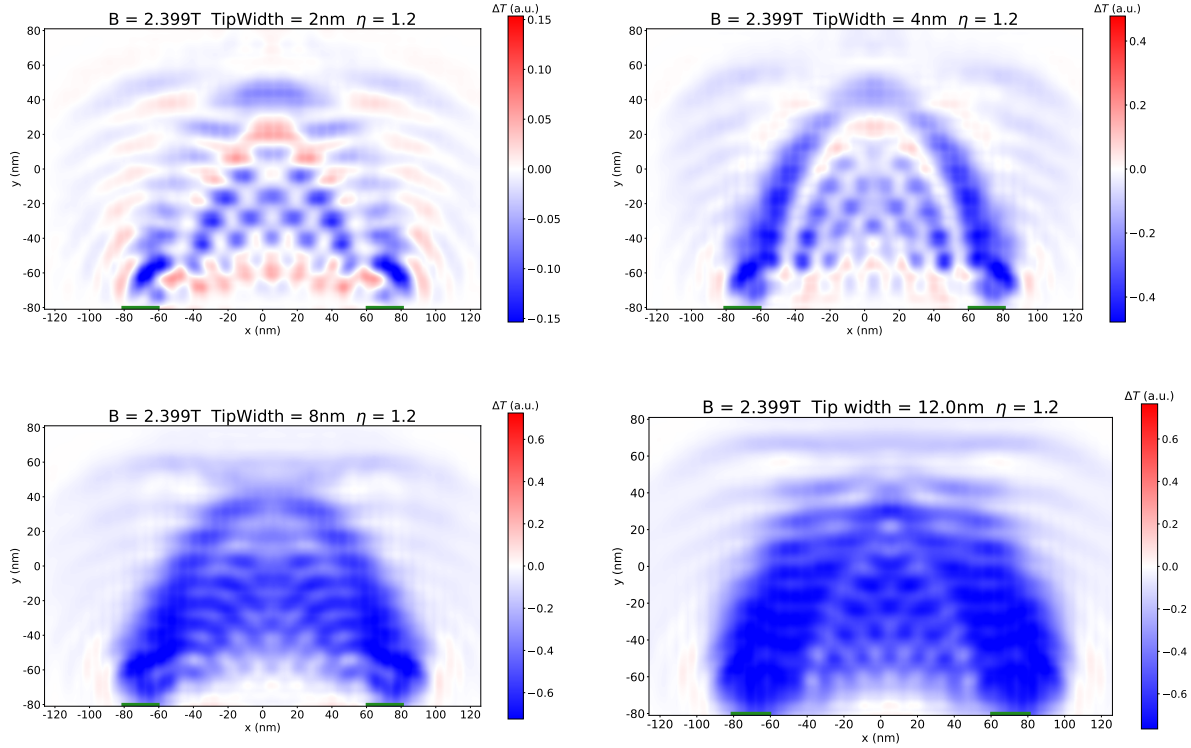


Figure 4.3: One mode - first resonance - $\eta = 1.2$ - variation tip width

Variation of η with a tip width of 2 nm When using a small tip width, increasing the strength of the probe does not change the pattern in the SGM image. This is shown in Figure 4.4 where η is progressively increased while the tip width is kept constant at 2 nm. The major change is the magnitude of ΔT as seen from the different colorbars. In order to respect the theory mentioned above, the fringes of the pattern should come closer to each other as η increases. Our results are thus in contradiction with this prediction. Moreover, it seems that two sets of fringes are present: a first one where blue and red regions alternate and are parallel to the expected classical cyclotron orbit and a second one of alternating red (or blue) and white zones more or less perpendicular to the orbit. We could not explain this second set and [1] does not mention such phenomenon. The tip width being very small might be a beginning of explanation since it is even smaller than the wavelength of the electrons. This implies that they are not strongly affected by the probe since they do not "see" it.

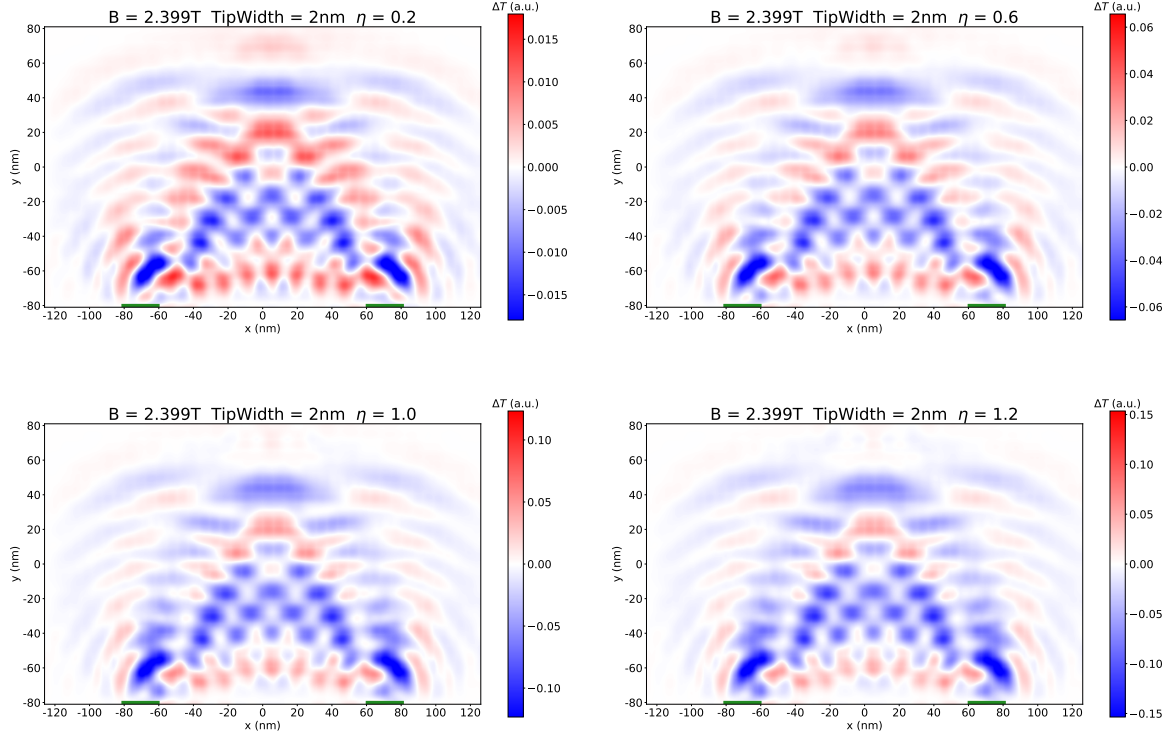


Figure 4.4: One mode - first resonance - tip width = 2 nm - variation of η

Variation of η with a tip width of 12 nm The influence of the tip strength with a large tip can be observed in Figure 4.5.

Although not perfectly distinguishable, the classical cyclotron orbit is more visible for the weak ($\eta = 0.2$) and the moderate ($\eta = 0.6$) tips. This is indeed what is expected because the tip reflects the electrons with a small angle, giving a large fringe spacing which is not visible on the images. For the strongest tips ($\eta = 1.0, 1.2$), the interferences appear because of backscattering as previously discussed. It can be noticed that the cyclotron orbit is still visible.

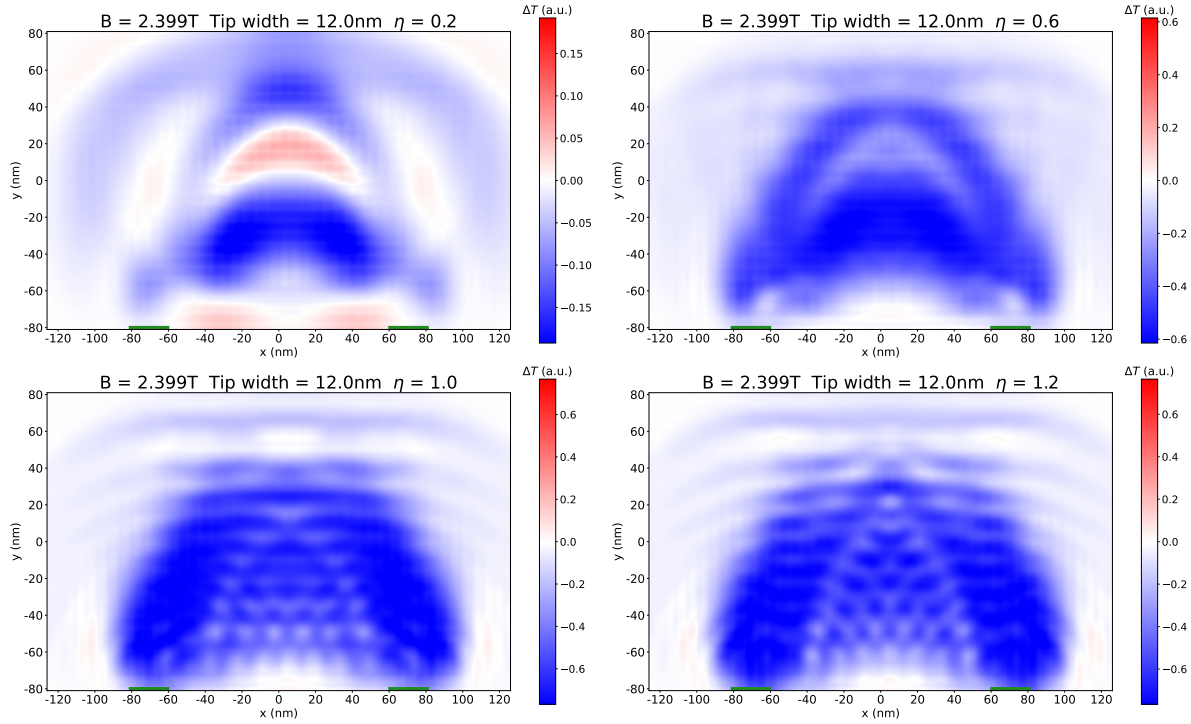


Figure 4.5: One mode - first resonance - tip width = 12 nm - variation of η

4.2.2 Second resonance - $B = 4.94\text{T}$

When the magnetic field is further increased to the second resonance, the electrons bounce back on the sidewall allowing them to reach the second QPC.

Now that the effects of the size and strength of the tip on the images has been emphasized, only the extreme cases are studied ($\eta = 0.2, 1.2$ and tip widths = 2, 12 nm).

As was expected, based on the previous section, the small and weak tip allows to see interferences. The large and weak tip allows to see the classical trajectory but seems to tell that the electrons are bouncing back two times on the sidewall before reaching the second QPC while they bounce only one time, as suggested by the current maps. Moreover, this image shows an increase in transmission just above the two QPCs and at half distance between them. Since the electrons are expected to be at these positions, it is not expected to have an increase in transmission there. The two other images are even more difficult to interpret, especially the one with the large and strong tip which show unclear interferences.

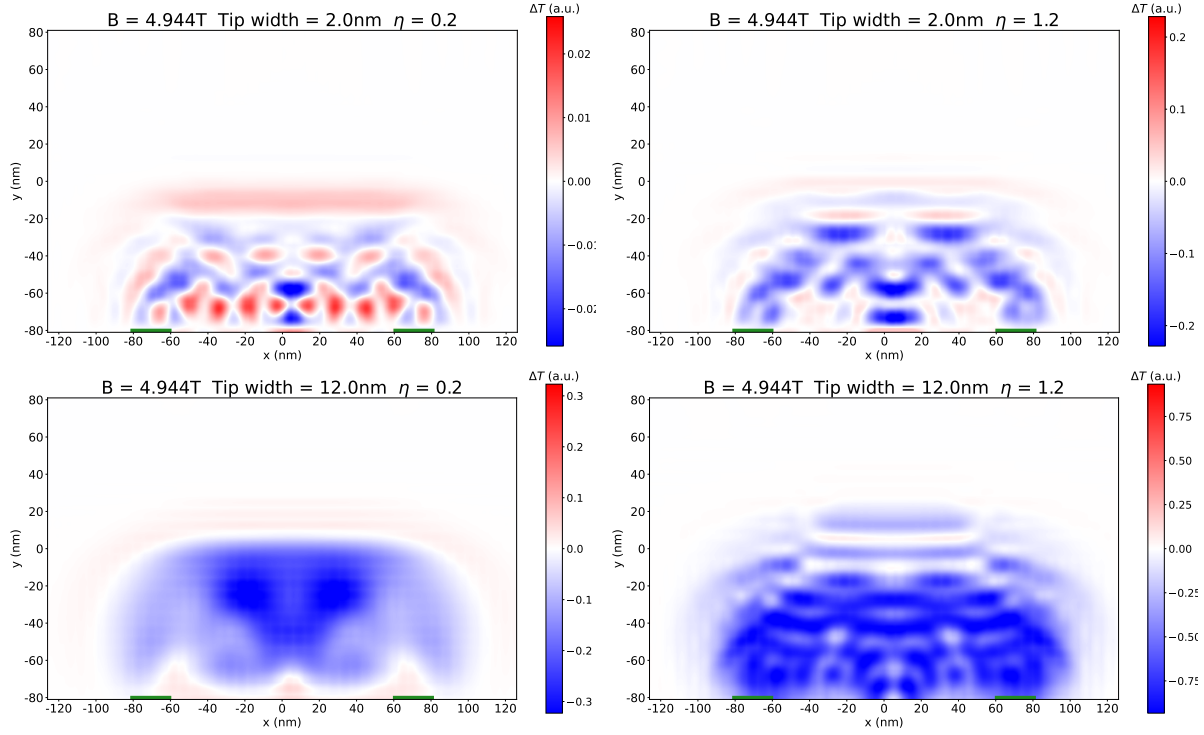


Figure 4.6: One mode - second resonance.

5 System without disorder - 2 modes in the QPCs

When the Fermi level is raised to $E_F = 0.15 \cdot t$, 2 modes are allowed in the QPCs. This additional mode leads to new interferences and thus new patterns in the SGM images. Indeed, the mode I (resp. mode II) in the first QPC can be transmitted in the mode II (resp. mode I) of the second QPC, as considered in the Landauer-Büttiker formalism.

As a reminder, $B_1 \propto \sqrt{E_F}$, meaning the resonant magnetic fields are expected to be larger when modes are added. This relationship also highlights the fact that one cannot study a system with many modes. Indeed, the quantum Hall effect will appear at higher magnetic fields which will lead to the apparition of edge channels. This is of course not desired for studying magnetic focusing.

5.1 Transmission as a function of the magnetic field

Figure 5.1 plots the transmission when the magnetic field is varied from 0 T to 10.6 T. Two peaks are visible at 3.53 T and 7.21 T (the other peak at 6.77 T has a slightly smaller transmission). They are associated to the two first resonances and will be studied in the following sections. In a similar way to the case with 1 mode, the resonant magnetic fields are smaller than the computed ones with Equation 3.3 but respects well the proportionality $B_2 \approx 2 \cdot B_1$. The estimations of Equation 3.3 multiplied by the factor 0.839 are 3.56 T and 7.13 T which fit pretty well the correct values.

A video of the current map with increasing magnetic field in this situation can be found at https://github.com/VicTrqt/LELEC2710---Nanoelectronics---Project-Aidala/blob/main/2%20Modes/Video_NoDisorder_2modes.avi.

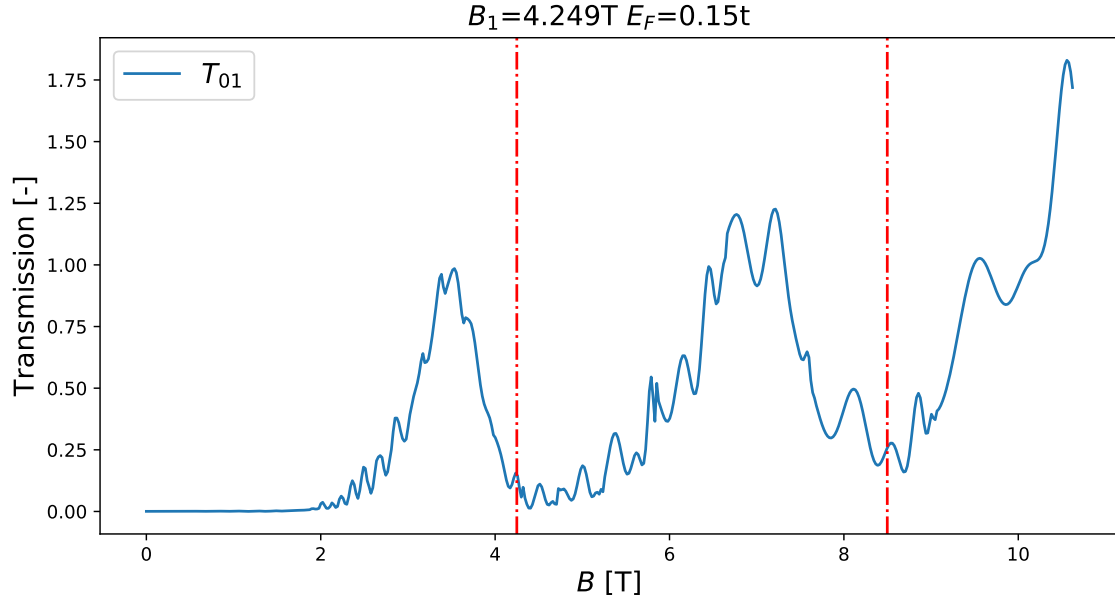


Figure 5.1: Transmission as a function of the magnetic field for a system without disorder and 2 modes in the QPCs. The theoretically calculated resonant magnetic fields are represented by the vertical dot-and-dashed red lines. E_F refers to the Fermi level while B_1 is the predicted magnetic field at the first resonance via Equation 3.3.

5.2 SGM images

5.2.1 First resonance - $B = 3.53 \text{ T}$

Figure 5.2 shows the SGM images of all four extreme cases when 2 modes are allowed and for the first resonant field.

As expected and mentioned, the only noticeable difference with the first resonance-1 mode SGM images of same tip width and strength is the different interference pattern.

Since E_F is raised compared to the case with one mode, λ_F is decreased to $\lambda = 16.22 \text{ nm}$. The strength of the tip is still $\sim 0.4 \cdot V$ at this distance. Therefore, the electrons in the case with two modes interact more with the tip than the ones with only one mode.

Other than that, the same conclusions can be reached regarding the influence of the tip width and strength.

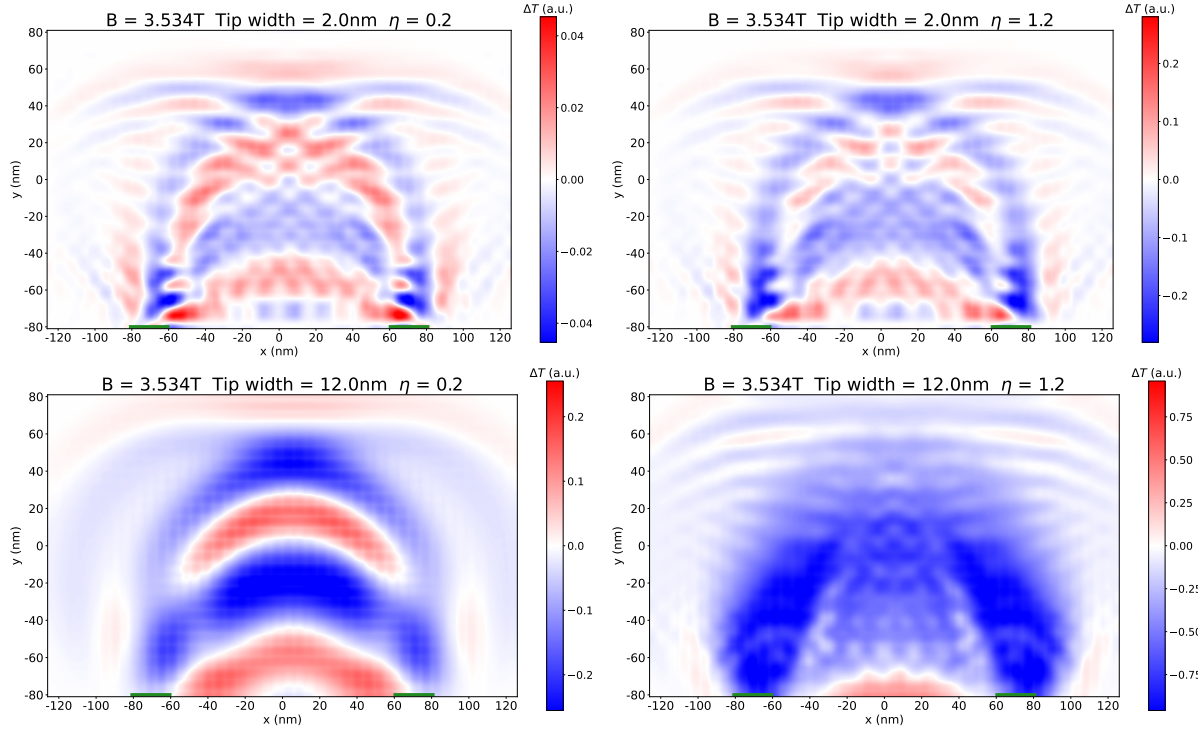


Figure 5.2: Two modes - first resonance

5.2.2 Second resonance - $B = 7.22\text{ T}$

Figure 5.3 shows the SGM images of all four extreme cases when 2 modes are allowed and for the first resonant field.

A disturbing feature of the $\eta = 0.2$ images is that, according to our interpretation so far, no electrons seem to bounce on the wall in-between the QPCs. This problem is thankfully solved by increasing the tip widths. However, the trajectory is still not as expected since we recover this positive ΔT just at the middle of the wall, where the electrons should bounce. This feature was already present in the 1 mode situation.

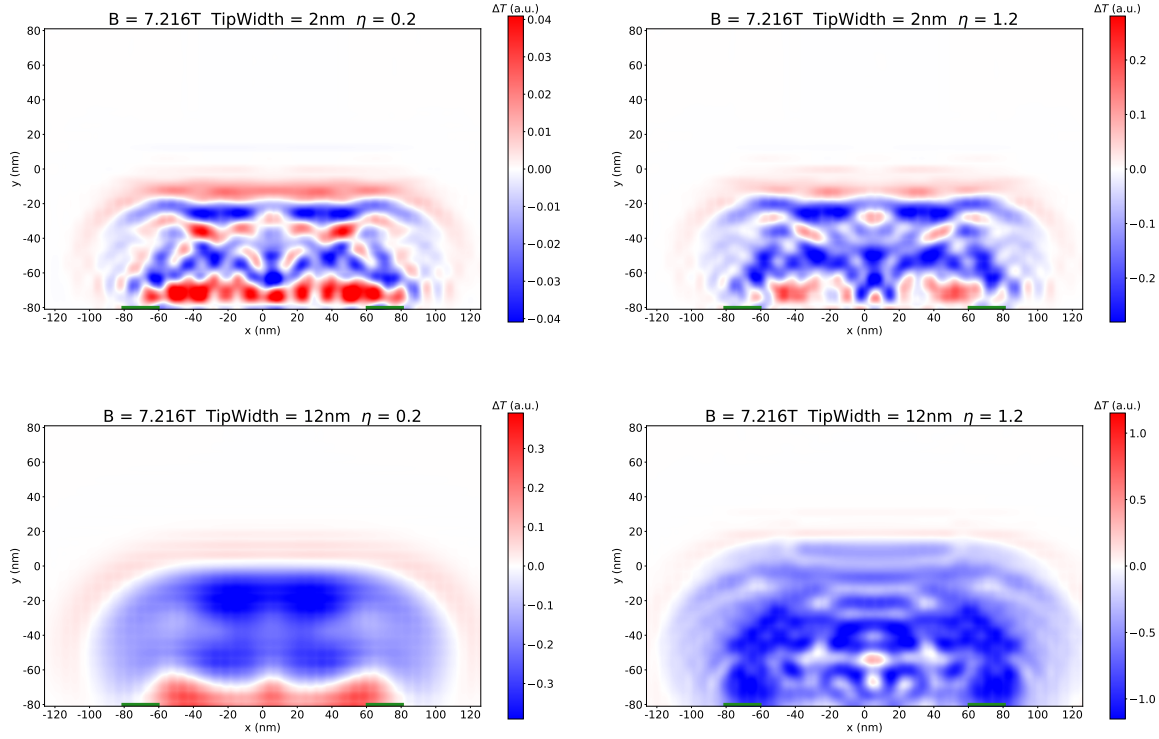


Figure 5.3: Two modes - second resonance

5.2.3 Current Maps

As mentioned, negative changes (blue regions) of transmission should imply that less current reaches the second QPC when the tip is placed at this location of the sample. The inverse reasoning should be valid for red regions. In order to verify the correctness of this assumption, one can superimpose the current stream lines onto SGM images and can try to detect changes in the current map once a tip is introduced in the system. Figure 5.4 illustrates this process. The 2 modes case with a tip width of 12 nm and η of 0.2 was chosen because it displayed a high enough contrast, both in the red and the blue areas as shows Figure 5.4a without the tip. As one can see from the neighboring images, no clear deviations related to the introduction of the tip is visible at first glance. Although slight changes can be noticed (see highlighted lines), it is difficult to say for certainty that these are a direct translation of the drop or augmentation of the transmission. Those red lines were indeed drawn as a mean to show lines that are different from the ones of Figure 5.4a and that have the right behavior with respect to the sign of ΔT . However, this latter might be too low in comparison to the transmission (about 20%) to produce a clear difference in trend.

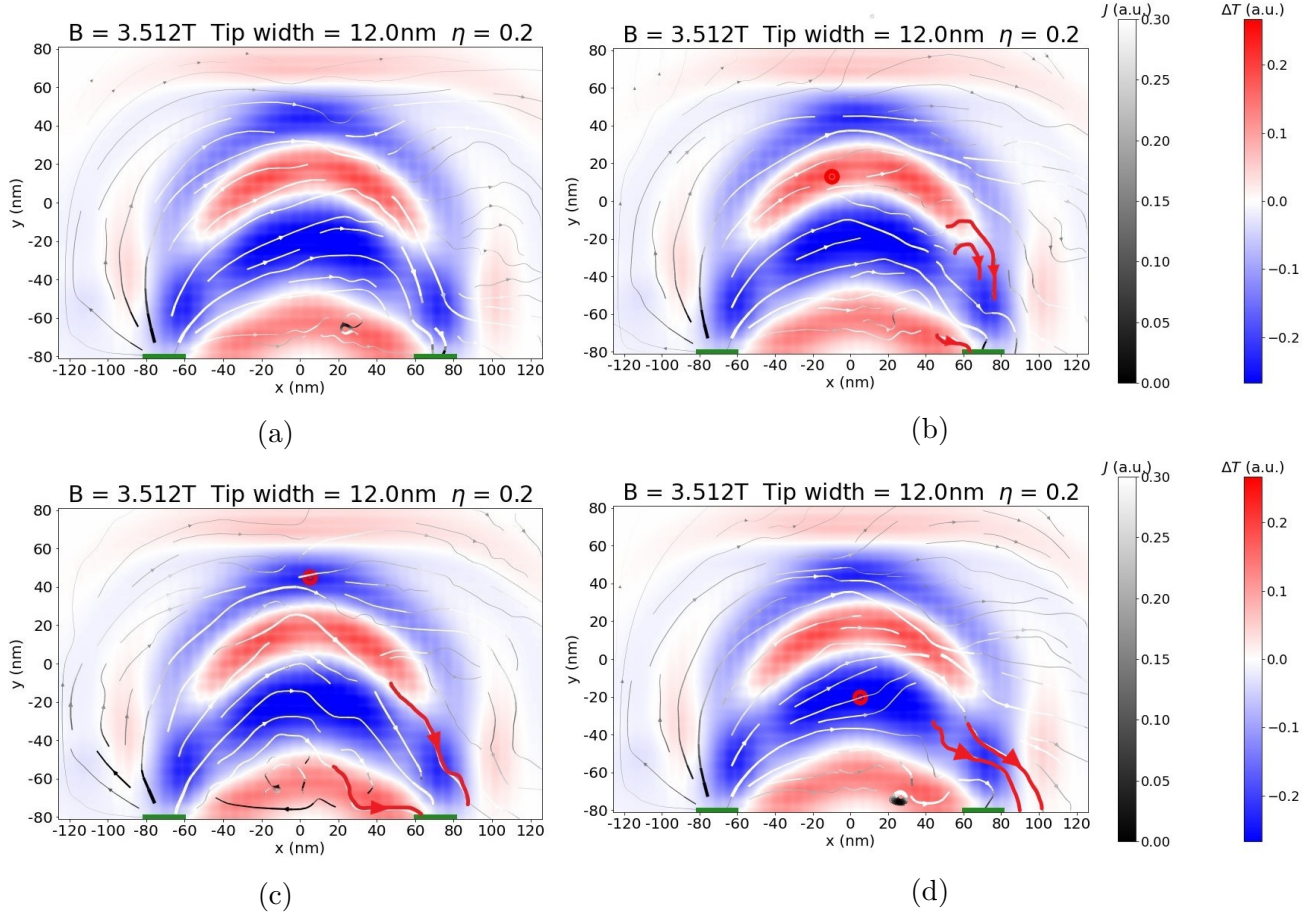


Figure 5.4: Two modes, second resonance, current maps superimposed, interesting streams are highlighted in red and the tip position is indicated by two concentric and thick red circles. (a) is the original map without any tip (see text).

As a last attempt to visualize the effect of the tip, the initial current was subtracted from the one in the presence of the tip ($J_{Tip} - J_{noTip}$) and the result was again plotted onto the SGM images (see Figure 5.5). As previously, interesting stream lines were highlighted because of their directions in accordance to the sign of ΔT . It seems that this analysis is a bit more fruitful than the previous one. Although not that dominant, clearer trends can be identified in Figure 5.5b and Figure 5.5c in the case of destructive interference. Figure 5.5a is less positive as only two arrows were highlighted. This could also be explained by $|\Delta T|$ being too small to cause any noticeable change. Another limitation is the way *matplotlib streamplot* works. It actually chooses randomly the beginning of the arrows. It is probably possible to customize this function in order to plot more arrows near the second QPCs but this has not been done due to time constraints.

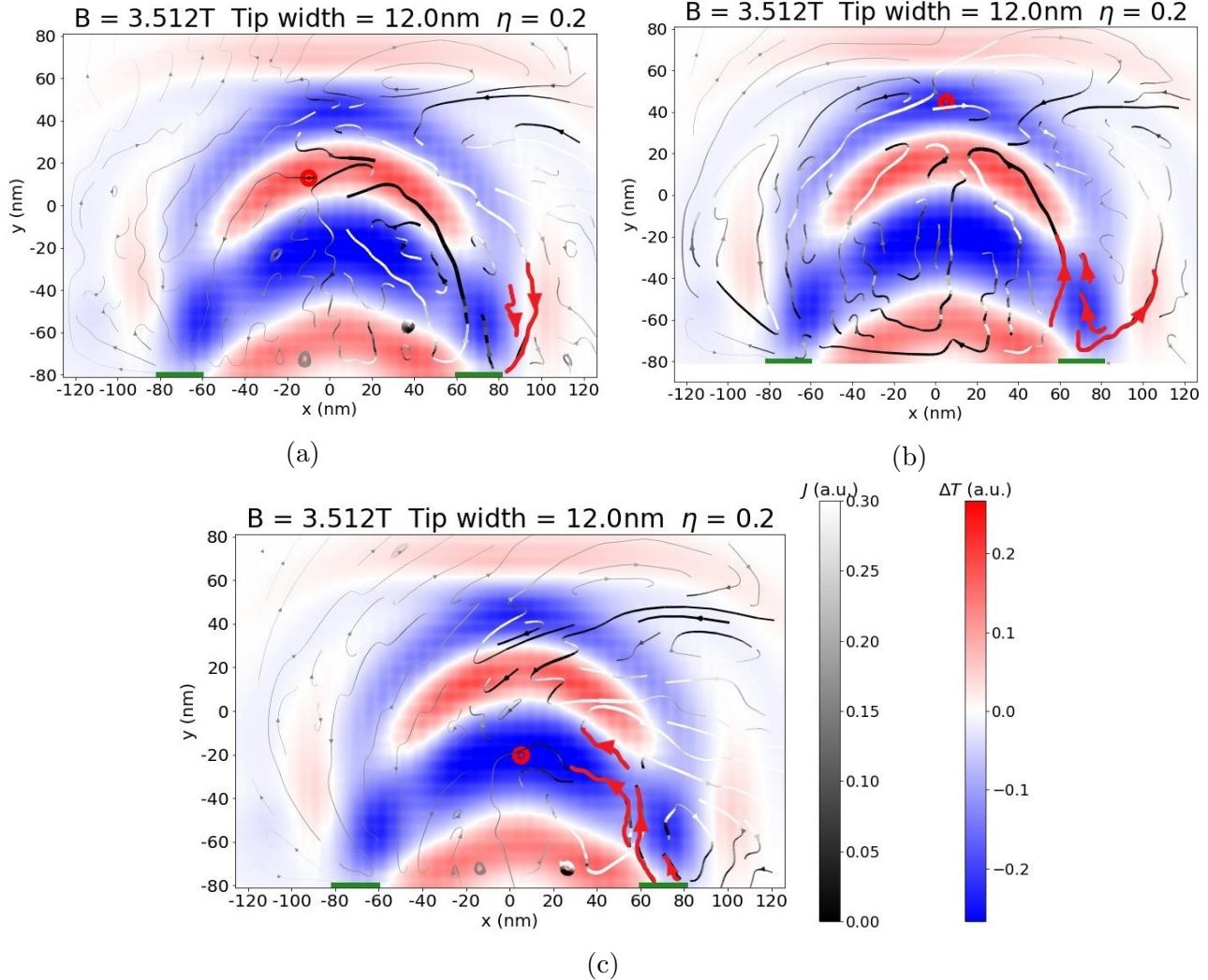


Figure 5.5: Two modes, second resonance, $J_{Tip} - J_{noTip}$ superimposed on SGM images, interesting streams are highlighted in red and the tip position is indicated by two concentric and thick red circles. The tip positions and system are the same as in Figure 5.4.

6 System with disorder - 1 mode in the QPCs

In real systems, one always has neutral and charged impurities, defects, etc. Aiming for more realistic simulations, it is thus interesting to introduce relatively random and reproducible disorder in the system. This is exactly what provides the *digest* package from *Kwant*. This latter allows us to apply a random gaussian disorder. It can also apply a uniformly random one but this would not reflect well reality and was thus not chosen.

The introduced disorder at the different positions of the sample is,

$$\text{Disorder}(x, y) = \text{Random gaussian disorder}(x, y) \times E_F \quad (6.1)$$

where the random gaussian disorder generates a value between 0 and 1 at each position (x, y) ,

following the probabilities of a gaussian distribution.

6.1 Transmission as a function of the magnetic field

Figure 6.1 plots the transmission when the magnetic field is varied from 0 T to 7.3 T. Two peaks are visible at 2.52 T and 5.03 T. They are associated to the two first resonances and will be studied in the following sections. In a similar way to the case without disorder, the resonant magnetic fields are smaller than the computed ones with Equation 3.3 but respects well the proportionality $B_2 \approx 2 \cdot B_1$. The estimations of Equation 3.3 multiplied by the factor 0.839 are 2.44 T and 4.87 T, which again fit well the correct values.

A video of the current map with increasing magnetic field in this situation can be found at https://github.com/VicTrqt/LELEC2710---Nanoelectronics---Project-Aidala/blob/main/1%20Mode%20with%20disorder/Video_Disorder_1mode.avi.

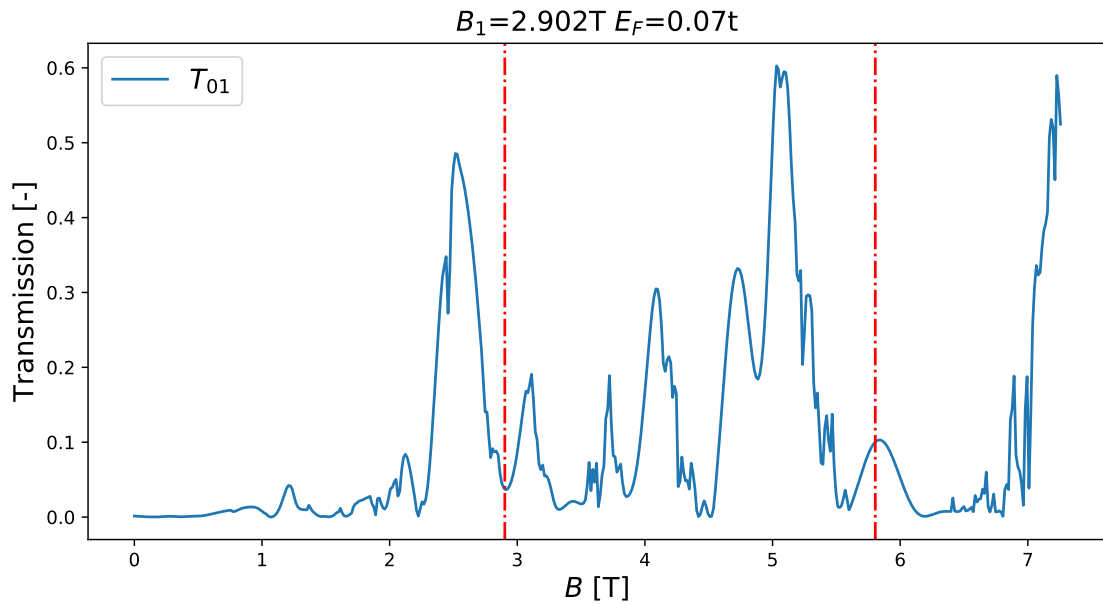


Figure 6.1: Transmission as a function of the magnetic field for a system with disorder and 1 mode in the QPCs. The theoretically calculated resonant magnetic fields are represented by the vertical dot-and-dashed red lines.

6.2 SGM images

6.2.1 First resonance - $B = 2.52$ T

Figure 6.2 shows the SGM images of all four extreme cases when 2 modes are allowed and for the first resonant field.

A branched flow was clearly observed in the video presenting the current density at different magnetic fields. This branched flow was still expected for the SGM images but it is not present,

or difficult to distinguish.

The presence of disorder has drastically changed the images, so that it is impossible to find the classical cyclotron orbit. The most appropriate tip for seeing this orbit without disorder was the tip width of 12 nm with $\eta = 0.2$. Here, it does show a cyclotron orbit anymore but still, a new path seems to emerge and leads to the second QPC.

Because of the disorder, the interferences do not have a symmetric pattern anymore and are quite difficult to interpret. Finally, the tip width of 12 nm with $\eta = 1.2$ still presents some interferences but again, no clear pattern is emerging from it.

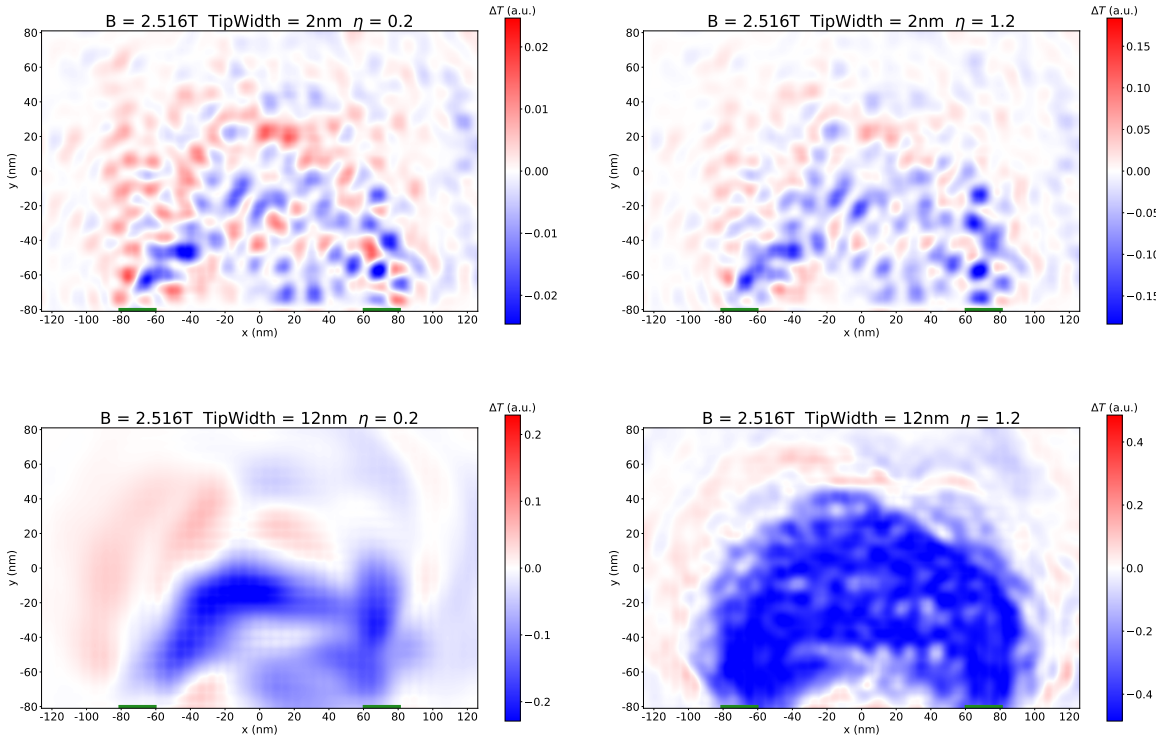


Figure 6.2: One mode - second resonance

6.2.2 Second resonance - $B = 5.03 \text{ T}$

Figure 6.3 shows the SGM images of all four extreme cases when 2 modes are allowed and for the second resonant field.

Again, both the interferences and the classical cyclotron orbit are difficult to interpret and distinguish in these images.

Other images, with a lower disorder than Equation 6.1, would probably be useful to study more in depth the effect of disorder. However, this is not done here.

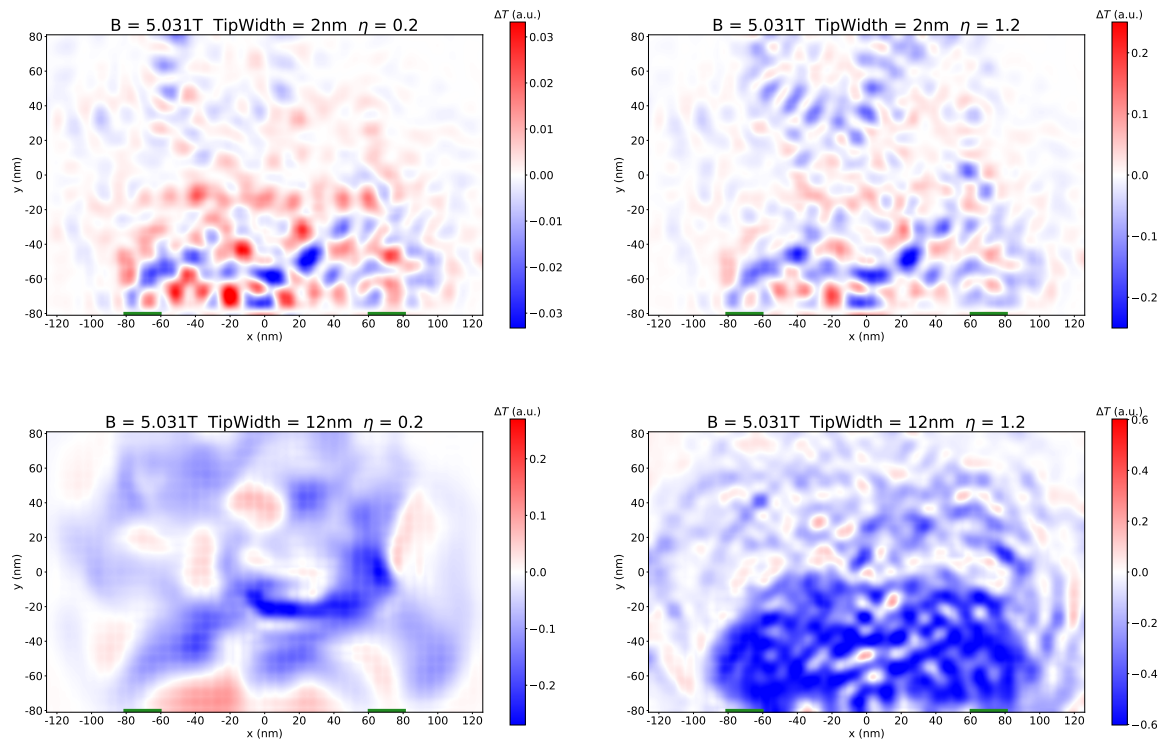


Figure 6.3: One mode - second resonance

7 Conclusion

The aim of this report was to obtain images of the magnetic focusing of coherent electrons waves, using the framework of the tight-binding model provided by *Kwant*.

The first step was to determine the Fermi level E_F by selecting 1 or 2 modes in the leads. According to Equation 3.3, the resonant magnetic fields increase when the Fermi level is raised, and so it does when increasing the number of modes. Therefore, the magnetic field can become sufficiently large for the apparition of channels due to the quantum Hall effect, which is not desired here. This explains why this report did not present results for a large number of modes. Only the qualitative change due to an additional mode was of interest.

The second step was to plot the transmission as a function of the magnetic field in order to find the resonant magnetic fields which have the highest transmissions. It has been found that, in each case, the resonant magnetic fields were systematically smaller than the one provided by Equation 3.3. However, this equation can compute the correct values if it is multiplied by a corrective factor equal to 0.839. This factor can be determined more precisely by taking the average correction for many resonant fields.

The third step was to obtain images of the system. Two different methods were used, the first using the current map and the second using the principle of the SGM. The former allowed to make videos showing where the current was going and a branching flow after introducing a gaussian disorder, while the latter allowed to study the classical cyclotron orbit as could be obtained by a real setup. The interferences arising from the coherent electron waves are also visible in the SGM images.

For the SGM images, the effect of the size and strength of the tip have been studied. As predicted in [1], the tip width of 12 nm with $\eta = 1.2$ provided images allowing to study the interferences due to the backscattering while the tip width of 12 nm with $\eta = 0.2$ provided images showing the classical cyclotron orbit. However, the interferences present on the images with a small tip of 2 nm remain unclear.

In conclusion, the simulations of this report are in agreement with the ones presented in [1] and raise new questions about the influence of the width of the tip.

References

1. Aidala, K. E. *et al.* Imaging magnetic focusing of coherent electron waves. *Nature Physics* **3**, 464–468. ISSN: 1745-2481. <https://doi.org/10.1038/nphys628> (July 2007).